The Astrophysical Journal, 747:108 (7pp), 2012 March 10 doi:10.1088/0004-637X/747/2/108

ASTEROSEISMOLOGY OF THE NEARBY SN-II PROGENITOR: RIGEL. I. THE *MOST* HIGH-PRECISION PHOTOMETRY AND RADIAL VELOCITY MONITORING*

Ehsan Moravveji[1,2], Edward F. Guinan[2], Matt Shultz[3], Michael H. Williamson[4], and Andres Moya[5]
[1] Department of Physics, Institute for Advanced Studies in Basic Sciences (IASBS), Zanjan 45137-66731, Iran; moravveji@iasbs.ac.ir
[2] Department of Astronomy, Villanova University, 800 Lancaster Avenue, Villanova, PA 19085, USA
[3] Royal Military College of Canada, PO Box 17000, Station Forces, Kingston, ON K7K 4B4, Canada
[4] Center of Excellence in Information Systems, Tennessee State University, Nashville, TN, USA
[5] Departamento de Astrofísica, Centro de Astrobiología (INTA-CSIC), PO BOX 78, 28691 Villanueva de la Cañada, Madrid, Spain
Received 2011 October 6; accepted 2011 December 21; published 2012 February 22

ABSTRACT

Rigel (β Ori, B8 Ia) is a nearby blue supergiant displaying α Cyg type variability, and is one of the nearest Type II supernova progenitors. As such it is an excellent test bed to study the internal structure of pre-core-collapse stars. In this study, for the first time, we present 28 days of high-precision *MOST* photometry and over six years of spectroscopic monitoring. We report 19 significant pulsation modes of signal-to-noise ratio, S/N $\gtrsim$ 4.6 from radial velocities, with variability timescales ranging from 1.21 to 74.7 days, which are associated with high-order low-degree gravity modes. While the radial velocity variations show a degree of correlation with the flux changes, there is no clear interplay between the equivalent widths of different metallic and Hα lines.

Key words: asteroseismology – spectroscopic – stars: individual: Rigel – Sun: oscillations – supergiants

Online-only material: color figures, machine-readable tables

1. INTRODUCTION

Blue supergiants (BSGs) such as Rigel are post-main-sequence (MS) massive stars ($M \gtrsim 15\,M_{\odot}$) evolving quickly across the Hertzsprung–Russel diagram. They are among the most intensively studied objects in contemporary astrophysics (see Maeder & Meynet 2011 for a recent review). BSG stars are intriguing objects because they end their lives as Type II supernovae (SN-II) which serve as catalysts for star formation and primary contributors to the heating and chemical enrichment of their host galaxies. These stars also offer a potentially valuable addition to the distance ladder through the BSG wind-momentum–luminosity (Kudritzki et al. 1999) and flux-weighted gravity–luminosity relationships (Kudritzki et al. 2003) which give very consistent distance determinations to the Local Group of galaxies (Kudritzki et al. 2008; U et al. 2009).

Fascinating features of BSGs include their microvariability in flux (e.g., Sterken 1977), complex changes in radial velocity (RV), as well as variations in the equivalent widths (EW) and line profiles of Balmer (especially Hα) and metallic lines (Kaufer et al. 1996, 1997; Richardson et al. 2011). Kaufer and coworkers monitored the optical spectra of six BA supergiants (including Rigel and α Cyg). They analyzed the RV measures of these stars and associated their observed variability with non-radial pulsations since the traveling features in the dynamical spectra could not be reconciled with the rotational periods of the stars. Waelkens et al. (1998) discovered 32 pulsating BSGs in the *Hipparcos* database which belong to the α Cyg class of variable stars, with periods ranging from 1.5 to 24 days. They were later definitely identified as gravity mode oscillations by a non-LTE spectroscopic analysis of Lefever et al. (2007) who compared the current position of their stars with the instability strip of g-mode dominated pulsators. Beyond the Milky Way, Bresolin et al. (2004) detected a handful of variable BSGs in NGC 300 and found the periods of two of these stars to be 72.5 and 96 days. Recently, Aerts et al. (2010b) correlated the sudden amplitude decline in the spectroscopically peculiar *CoRoT* target HD 50064 (B1-6 Ia) to radial *strange mode* variability with a 37 day period; they inferred a mass of $\sim$45 $M_{\odot}$ for this luminous mass-losing BSG. Despite several decades of observational efforts on ground-based photometry and spectroscopy of α Cyg type pulsating stars, it is not certain what portion of their variability is periodic, or how far they deviate from strict periodicity.

The nature of the aforementioned variability in high-mass post-MS variables is still poorly understood. The photometric variability of HD 163899 (B2 Ib/II) found by *MOST* (*Microvariability and Oscillations of Stars*) observations revealed a total of 48 pressure (p) and gravity (g) modes. Saio et al. (2006) showed that these modes can be simultaneously excited by the κ-mechanism and reach the surface if they arrive at the base of the intermediate convection zone (ICZ) with an appropriate phase. Gautschy (2009) searched for the origin of long-period variabilities in the prototype α Cyg. Interestingly his Figure 5 shows a gap where no instabilities are predicted for evolutionary tracks with $3.95 \lesssim \log T_{\rm eff} \lesssim 4.15$. Rigel lies in this gap. In contrast to this result, the study of Saio (2011) predicts that Rigel should be unstable against non-radial convective g^- modes. This contradiction could arise from different physical ingredients (such as rotational and overshoot mixing) and various numerical techniques in pulsation codes. This is not surprising since evolved massive stars like Rigel are demanding to model.

The radial strange mode is proposed as another mechanism to induce instability and interplay with mass-loss efficiencies in these massive stars with $\log(L/M) \gtrsim 4\log(L_{\odot}/M_{\odot})$ (see, e.g., Dziembowski & Slawinska 2005; Saio 2011; Aerts et al. 2010b, and references therein). This requirement is also marginally fulfilled by Rigel. Godart et al. (2009) investigated the destructive impact of core overshooting and mass loss during the MS lifetime on the extent of the ICZ, and showed that models with wider ICZs are more likely to destabilize stellar

* Based on data from the *MOST* satellite, a Canadian Space Agency mission, operated jointly by Dynacon, Inc., the University of Toronto Institute of Aerospace Studies, and the University of British Columbia, with the assistance of the University of Vienna.

oscillations. These studies show that asteroseismology of slowly pulsating BSGs can reveal a wealth of information about the internal structure of SN-II progenitors. This can be complementary to the understanding of the physical properties of pulsars which originate from the cores of massive stars (Heger et al. 2005).

This is the first paper in a series of investigations aiming at probing the details of the internal structure of BSGs through asteroseismic study, and investigating the origin of their short- and long-period variability. Rigel was selected as an ideal test subject because of its apparent brightness, proximity, and current evolutionary status. The latest measurements of the physical parameters of Rigel collected from the literature are summarized in Section 2. The space-based *MOST* photometry and ground-based spectroscopy are presented in Section 3. The results of the multimode pulsation frequencies are finally discussed in Section 4. The interpretation of the pulsation frequencies will appear in E. Moravveji et al. (in preparation).

2. ABOUT RIGEL

Rigel (β Ori; HD 34085; B8 Ia; $V \sim 0.12$ mag) is the sixth-brightest star in the night sky and the most luminous star in the solar neighborhood. It is a member of a multiple star system where its companion, Rigel B, is a spectroscopic binary about $9\farcs5$ distant (Sanford 1942). From the revised *Hipparcos* parallax the distance to Rigel is $d_{\rm Hip} = 264 \pm 24$ pc (van Leeuwen 2007) which is smaller than the 360 ± 40 pc adopted by Hoffleit & Jaschek (1982) who assumed that Rigel originates from the τ Ori R1 complex.

Fundamental parameters of Rigel which impose valuable constraints on the equilibrium model of the star are already measured. They are effective temperatures $T_{\rm eff} = 12{,}100 \pm 150$ K, surface gravity $\log g = 1.75 \pm 0.10$, luminosity $\log(L/L_\odot) = 5.08^{+0.07}_{-0.10}$, near-solar metallicity $[M/{\rm H}] = -0.06 \pm 0.10$, surface He abundance $Y_{\rm s} = 0.32 \pm 0.04$, and $v \sin i \approx 25 \pm 3$ km s^{-1} (Przybilla et al. 2006, 2010; Simón-Díaz et al. 2010). The most up-to-date limb-darkened angular diameter for Rigel comes from CHARA/FLOUR K-band interferometry $\theta_{\rm LD} = 2.75 \pm 0.01$ mas (Aufdenberg et al. 2008) which in combination with $d_{\rm Hip}$ yields $R = 78.9 \pm 7.4\ R_\odot$. Przybilla et al. (2010) propose a mass of 23 $M_\odot$ from Geneva evolutionary tracks which include the effects of rotation.

The absolute bolometric magnitude is calculated (adopting the observed $B - V = -0.03$ from Nicolet (1978), and a bolometric correction BC $= -0.78$ from Bessell et al. 1998 with $E(B - V) = 0.05$ from Przybilla et al. 2006) to yield $M_{\rm bol} = -7.92 \pm 0.28$. By applying the flux-weighted gravity–luminosity relation of Kudritzki et al. (2003)

$$M_{\rm bol} = 3.71\ \log\left(g/T^4_{\rm eff,\,4}\right) - 13.49$$

($T_{\rm eff,\,4} = T_{\rm eff}/10{,}000$) which is optimized for BSGs, we arrive at a value of $M_{\rm bol} = -8.17 \pm 0.45$—in good agreement with our calculated value.

Moreover, Rigel's line profile variability in Hα (Kaufer et al. 1996; Morrison et al. 2008) and other metal-line EWs due to non-radial pulsations (Kaufer et al. 1997) and mass loss (Chesneau et al. 2010) is already published.

Rigel shows variations in the Hα spectral feature with some outburst events being recorded by Israelian et al. (1997) and O. Chesneau et al. (Very Large Telescope Interferometer (VLTI) campaign, in preparation). The morphology of this line is studied by Morrison et al. (2008). Moreover, Chesneau et al. (2010) detected an extended rotating Hα region from optical interferometry with VEGA/CHARA (Mourard et al. 2009) and speculate that Rigel is observed with its rotation axis along the north–south direction at significantly high inclination angle. They estimated that the current mass-loss rate is $\dot{M} = 1\text{–}2 \times 10^{-7}\ M_\odot$ yr^{-1}. Assuming a high inclination angle, the rotation velocity is well below 20% of the estimated critical breakup rotation rate of $\sim$185 km s^{-1} (Equation (2.19) in Maeder 2009), so spherical symmetry can be safely assumed for its geometry. The current best values of the physical parameters of Rigel are presented in Table 1. Additional parameters for Rigel are given by Przybilla et al. (2006). These are invaluable input for future seismic modeling and analysis.

Table 1
Updates to Physical Parameters of Rigel

Parameter	Value	Reference
$d_{\rm Hip}$ (pc)	264 ± 24	van Leeuwen 2007
$T_{\rm eff}$ (K)	$12{,}100 \pm 150$	Przybilla et al. 2010
$\log(L/L_\odot)$	$5.08^{+0.07}_{-0.10}$	This work
Y_s	0.32 ± 0.04	Przybilla et al. 2010
$v \sin i$ (km s^{-1})	25 ± 3	Przybilla et al. 2010
		Simón-Díaz et al. 2010
Inclination	$60^\circ \lesssim i \lesssim 90^\circ$	This work
$\theta_{\rm LD}$ (mas)	2.75 ± 0.01	Aufdenberg et al. 2008
$R/R_\odot$	78.9 ± 7.4	This work
$M_{\rm bol}$ (mag)	-7.92 ± 0.28	This work
$\dot{M}$ ($M_\odot$ yr^{-1})	$1\text{–}2 \times 10^{-7}$	Chesneau et al. 2010
B_d (G)	$\lesssim 25$	Shultz et al. 2011
$P_{\rm shortest}$ (d)	1.2191 ± 0.0001	This work
$P_{\rm longest}$ (d)	74.74 ± 0.28	This work

(This table is available in its entirety in machine-readable form in the online journal. A portion is shown here for guidance regarding its form and content.)

3. OBSERVATIONS

3.1. MOST High-precision Photometry

Rigel was observed continuously with the *MOST* satellite (Walker et al. 2003) for 27.7 days from 2009 November 15 to December 13. The data set consists of 30,640 observations after correcting for the Southern Atlantic Anomaly. Figure 1(a) shows the light curve after removing an offset of $\sim$0.12 mag. The abscissa is in HJD−2,450,000.0. Because of the brightness of the target, the precision of the observations is of the order of $\approx$0.05–0.10 mmag. Starting with a sinusoidal variability pattern, oscillations die out and Rigel seems quiescent for several days, approximately from HJD 5164 to 5168 (enlarged in Figure 1(b)), followed by a gradual rise, and a steep decline in light flux; this resembles a possible beating pattern and we expect close, low-frequency modes to appear in the harmonic analysis (Section 4). There is a 20 hr gap around HJD 5175, arising from an interruption in communication between the satellite and the ground station. This is at the time when the star is decreasing in brightness almost monotonically.

3.2. Spectroscopy

Rigel's optical spectrum has been monitored by the 2 m Tennessee State University Automatic Spectroscopic Telescope at Fairborn Observatory, AZ (TSU/AST; Eaton & Williamson 2007). A total of 2328 high-resolution ($R \sim 30{,}000$ and 20,000) moderate signal-to-noise ratio (S/N $\sim$ 50–150) echelle spectra

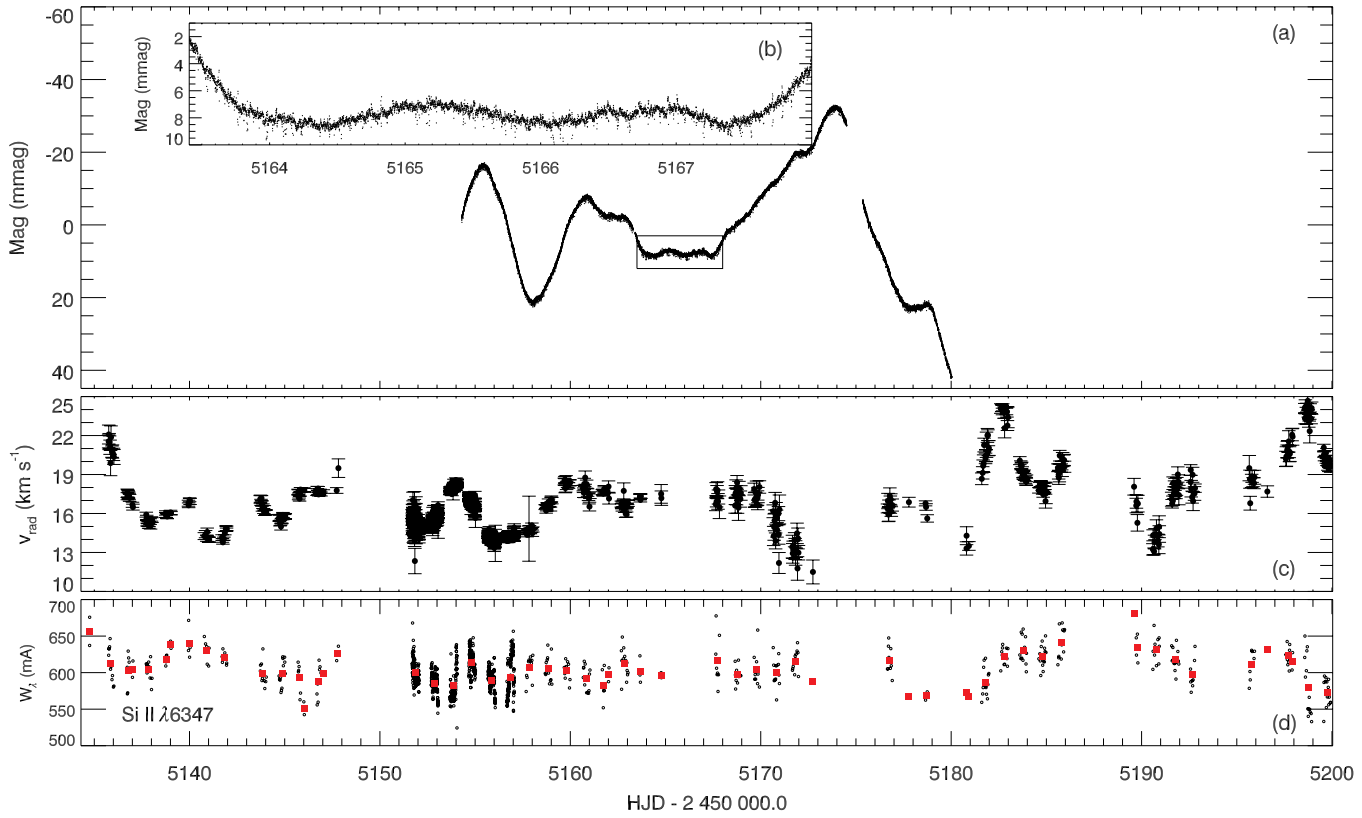

Figure 1. Compilation of observations from the Rigel campaign. Panel (a) shows the 27.7 day *MOST* space photometry (Section 3.1). Panel (b) is a five-day zoomed-in portion of the data to emphasize the amplitude and timescale of the shortest variations. Panel (c) shows the RV data which demonstrates a correlation with the flux changes (Section 3.2). Panel (d) is the equivalent width variation for Si II λ6347.1 during the same monitoring epoch (Section 3.4); the (red) squares are the one day binned averages (see Figure 2).

(A color version of this figure is available in the online journal.)

(4900–7100 Å) were obtained. The spectra were secured over 334 nights starting from 2003 December 11 to 2010 February 14. The density of time sampling was increased during the months centered on the *MOST* observations. Simultaneous with *MOST*, 442 spectra were collected over 20 nights.

The spectra were reduced at TSU by an automatic pipeline method without removing the telluric lines. The RV variations were derived by fitting a Gaussian to 29 metallic lines; Figure 1(c) shows the RV variations contemporaneous with *MOST* observations. An offset of +0.3 km s^{-1} was applied to the AST instrumental RV measurements (Eaton & Williamson 2007). The standard deviation in the mean for each RV measurement was evaluated as the standard deviation of the 29 measured absorption lines in each spectrum. Averaged over all spectra, this value is 0.26 km s^{-1}. In the years prior to the *MOST* observations, Rigel was observed sporadically with AST. Also, the AST data set is interrupted by cloudy weather that occurred during the *MOST* observing run. Thus the sampling is not even, and the analysis of these data will suffer from daily and annual aliasing.

Extensive and highly variable velocity changes are clearly visible in Figure 1(c). During the plotted interval, the RVs vary from 11 to 25 km s^{-1}. There is evidence for a correlation between the RV and *MOST* brightness variations. During this interval, and other seasons, the RV variations appear to exhibit complex periodicity typical of a multi-periodic pulsating star.

In addition to the AST spectroscopy, Rigel was observed with the VLTI during the time of the *MOST* observations. A preliminary analysis of the spectro-interferometry by O. Chesneau et al. (in preparation) shows that during this interval Rigel was relatively quiet, with the Hα line appearing in absorption with sometimes a weak emission component appearing at times, and no outbursts being recorded. No major high velocity absorption event is identified during this interval. This is confirmed by seven raw Ritter echelle spectra ($R = 26{,}000$, S/N 100–200) taken during the same interval at Ritter Observatory (N. D. Morrison 2011, private communication). As a result, there is no evidence of a possible propagating atmospheric shock or chaotic activity during *MOST* photometry.

3.3. Spectropolarimetry

In conjunction with *MOST* photometry, 78 observations were collected with the high-resolution ($R \sim 65{,}000$) spectropolarimeter ESPaDOnS, installed at the Canada–France–Hawaii Telescope, and its clone Narval at Telescope Bernard Lyot (TBL, Pic du Midi). Analysis with the multi-line cross-correlation technique least-squares deconvolution (Donati et al. 1997) reveals no evidence of a magnetic field (Shultz et al. 2011), with error bars on the longitudinal field B_l of the order of 15 G. Matching synthetic disk-integrated Stokes V profiles to the observed Stokes V profiles has constrained the dipolar magnetic field to be $B_d \lesssim 25$ G for high inclinations of the rotational axis and low obliquities of the magnetic axis, although $B_d \sim 50$ G is possible at low-intermediate inclinations, in which case the rotational period is shorter and fewer observations can be binned together (M. Shultz et al., in preparation). If, as discussed above, Rigel is viewed nearly equator-on, then the first of the conditions necessary for a higher upper limit applies. However, these upper limits cannot rule out the possibility of significant magnetic effects. Thus, in the absence of any positive evidence for a magnetic field, or any pressing theoretical reason to suspect

its existence, there is no reason at this time to complicate the pulsational analysis with its inclusion.

3.4. Equivalent Widths

Kaufer et al. (1997) showed that different spectroscopic lines in BA supergiants emerge from different optical depths τ_λ, in a sense that lines from shallower photospheric depths have larger equivalent widths (hereafter EWs designated by W_λ). They classified the lines in the optical band accordingly to weak (50 mÅ $\lesssim W_\lambda \lesssim$ 200 mÅ), medium (200 mÅ $\lesssim W_\lambda \lesssim$ 500 mÅ), and strong ($W_\lambda \gtrsim$ 500 mÅ). We chose C II λ6583 as a weak line, Hα, C II λ6578 and Si II λ6371 as medium lines, and He I λ6678 and Si II λ6347 as strong lines.

EWs of the above lines are calculated according to

$$W_\lambda = \int (1 - F_\lambda)\, d\lambda, \qquad (1)$$

where F_λ is the flux at each wavelength interval $d\lambda$, renormalized to the continuum on either side of the spectral line. To suppress the contribution from cosmic rays the spectra were filtered using a low-bandpass median filter; contamination from telluric lines was removed by identifying those regions so contaminated and using a higher-bandpass median filter. The corresponding errors for each EW measurement are evaluated with the per-pixel standard deviation of the flux from the mean value of a nearby section of the continuum and propagated through the measurement. Uncertainty in the location of the continuum is accounted for in the calculation of the per-pixel flux error from the S/N. As an example, Figure 1(d) shows the variations in W_λ for the Si II λ6347 line during the *MOST* photometry. There is a weak correlation between the RV and EW variations during this season, but it is not always present.

Comparison of ESPaDOnS/Narval spectra with contemporaneous AST spectra reveal that, while the instruments generally yield consistent measurements of W_λ, the comparatively lower-resolution AST spectra show a small but persistent bias in which W_λ systematically increases with the uncertainty $\sigma(W_\lambda)$. However, W_λ is accurate to within ∼5% which is sufficient to reveal at times a weak correlation between RV and the W_λ of, for instance, the Si II 6347 Å line, one of the stronger photospheric lines in the AST spectral window (see Figure 1(d)). Figure 2 is a 50 day representative interval, occurring one year prior to the *MOST* photometry, that shows the RV changes as a function of time (panel (a)). For the same time interval, panels (c) to (e) plot the EWs of five different lines. While Hα (having high sensitivity to wind) demonstrates the largest variation amplitude, the rest of the lines, though they have different absolute amplitudes, change moderately—on the order of 12%–19%. The two Si II lines follow a similar trend and have similar amplitudes.

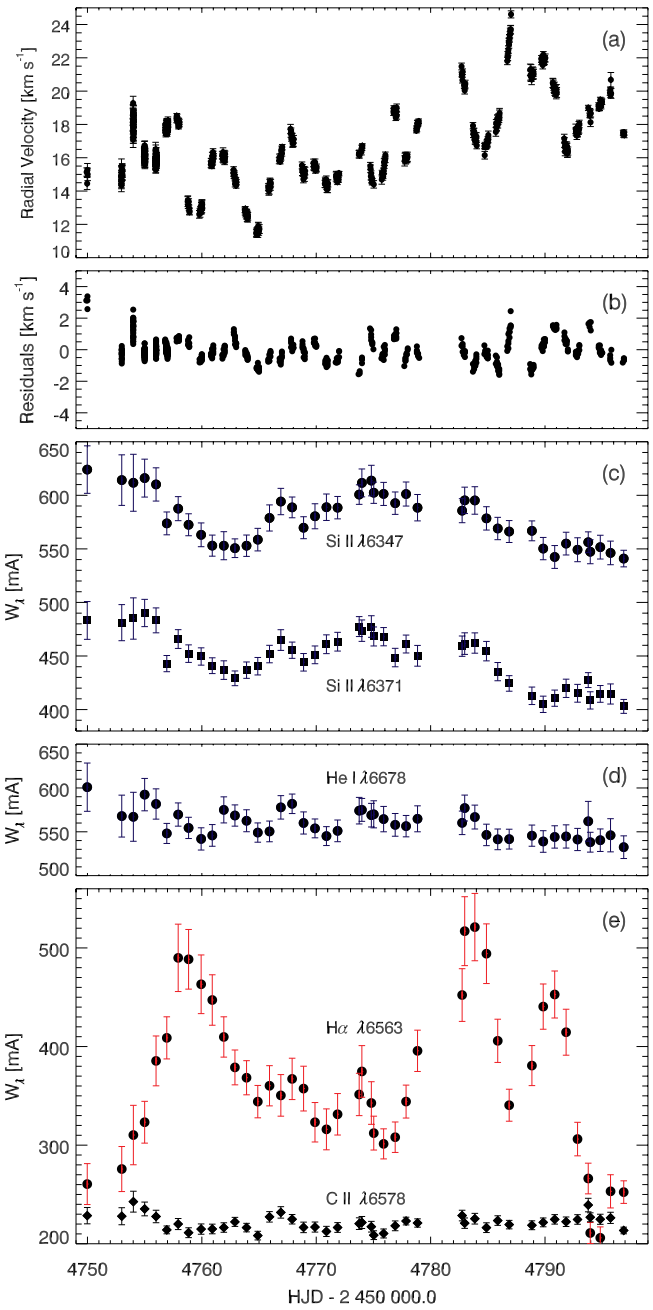

Figure 2. (a) Representative 50 day radial velocity curve of Rigel. 1σ error in RV is overplotted. (b) Residual plot with 19 harmonics removed as in Table 2 with rms deviation 0.59 km s^{-1}. (c) The one-day binned EW measures of two metallic lines, namely Si II λ 6347 and Si II λ 6371, which exhibit significant temporal variations. (d) A similar plot for the He I λ 6678 line, and (e) for C II λ 6578 and Hα lines.

(A color version of this figure is available in the online journal.)

4. RIGEL PERIODICITIES

4.1. Variability Pattern of Rigel

Kaufer et al. (1996, 1997) derived several harmonics to fit to the season-by-season photometry, RV, and EW variations of Rigel and five other late BA supergiants. As they demonstrated, the Hα line EWs show systematic variations. Figure 7 in Kaufer et al. (1997) shows that α Cyg, the prototype of this class of pulsating stars, and the other BSGs exhibit variability with periods exceeding a week. For the specific case of Rigel, the periods they find are in the range of 4 to more than 50 days. Richardson et al. (2011) found evidence for season-to-season changes in the oscillation frequencies of α Cyg (Deneb, A2 Ia) from five years of spectroscopic and photometric monitoring.

The need for multiple modes to fit to our RV and EW data set is clearly shown in Figure 2. Similar behavior is observed in other seasons. Because different spectral lines are formed at various optical depths of the star's atmosphere, the temporal changes in W_λ for strong lines (such as Si II λ6347) are significantly different from those of weak lines (such as C II λ6578). The EW, however, is sensitive to local changes in the effective temperature $\delta T_{\rm eff}/T_{\rm eff}$ and gravity $\delta g/g$. In a series of studies in β Cep and SPB stars (which are different from BA supergiants,

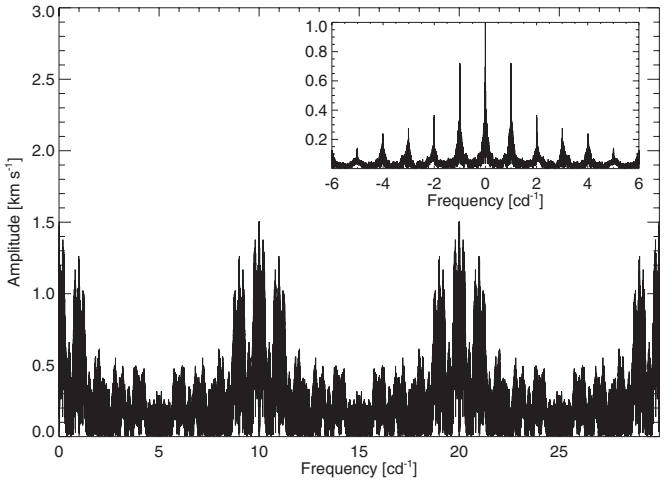

Figure 3. Discrete Fourier transform of the RV time series shows a repeating pattern at multiples of $f_{\rm nyq} = 5\,{\rm d}^{-1}$. The inner panel shows the spectral window and the one-day aliasing in addition to the annual aliasing.

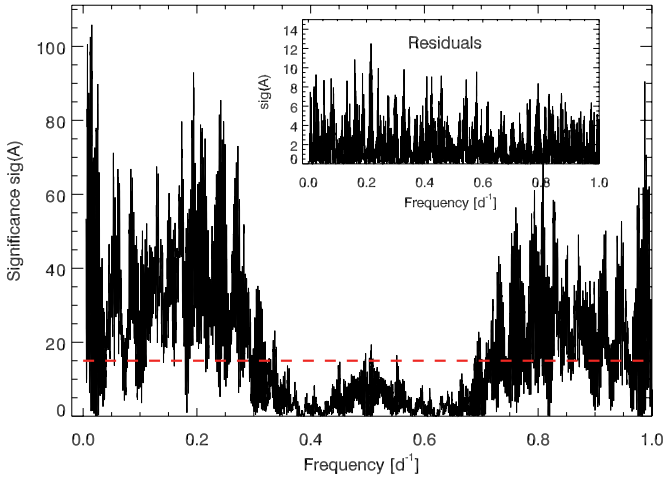

Figure 4. Significance spectrum of RV data with a normalized weight. Only the low-frequency domain between [0, 1] $\rm d^{-1}$ is shown. The inner panel shows the remaining power below the threshold sig = 15. After prewhitening of 19 significant harmonics, the residual is 0.94 km $\rm s^{-1}$.

(A color version of this figure is available in the online journal.)

but still have similarities in the nature of their pulsation), Dupret et al. (2002) and De Ridder et al. (2002) showed that a sinusoidal behavior in EW and RV time series with a common frequency is observed in only few cases. Given that Rigel (similar to SPBs) pulsates in g-modes which are transversal motions at the stellar surface, EWs are strongly affected by $\delta T_{\rm eff}/T_{\rm eff}$ (De Ridder et al. 2002). Based on the observed behavior of Rigel's EWs (panels (c) to (e) in Figure 2), we believe that a complex non-RV field exists across different optical depths (Aerts et al. 2009; Simón-Díaz et al. 2010). As Kaufer et al. (1997) showed (in their Figure 4), RV variations are negligibly affected by this depth dependence. Furthermore, the RV variations show a weak (not to say absent) degree of correlation with the EW of any of the lines.

4.2. Frequency Analysis Based on RV Data

Compared to the *MOST* photometry time series (Rayleigh limit of 0.036 $\rm d^{-1}$), the RV data have a much longer time span (Rayleigh limit of 4.43×10^{-4} $\rm d^{-1}$). As a result, we base our search for intrinsic signals primarily on this data set using two widely used state-of-the-art programs—`SigSpec` (Reegen 2007) and `Period04` (Lenz & Breger 2005). However, the RV data suffer from strong daily ($f_d = 1$ $\rm d^{-1}$) and annual ($f_a = 0.002769$ $\rm d^{-1}$) aliasing (inner panel in Figure 3). As shown in Figure 3, there is a repeating pattern every 5 $\rm d^{-1}$ in the discrete Fourier transform (DFT) spectra that arises from our sampling rate. Thus we selected the upper frequency scan range at $f_{\rm nyq} = 5$ $\rm d^{-1}$, and our analysis did not identify frequencies higher than 1 $\rm d^{-1}$.

`SigSpec` computes the spectral significance level (sig) for the DFT amplitude spectrum based on the analytical solution for the probability density function of an amplitude level of any peak during the iterative prewhitening process. By default the program scans for peaks with sig>5, which is approximately equivalent to S/N = 3.8 (Reegen 2007). However, we conservatively chose just to search for highly significant modes to avoid a forest of low-frequency peaks. To accomplish this, the prewhitening process is stopped if the significance (sig) of each peak or the cumulative significance (csig) of the whole solution is below 15. A similar threshold was used by Chapellier et al. (2011) in the frequency analysis of one of the *CoRoT* primary targets. Since each RV measurement i has an error σ_i, we associate a normalized weight $w_i = \sigma_i^{-2}/\sum_i \sigma_i^{-2}$ to each data point. The resulting significance spectrum is shown in Figure 4. This procedure leads to a prewhitening of 19 significant modes. The corresponding list of detected harmonics is presented in Table 2. It tabulates the multimode solution to the RV data set from `SigSpec`. Analytical 1σ uncertainties are evaluated according to Montgomery & Odonoghue (1999); those in Table 2 are 4σ uncertainties. After prewhitening, the rms of the residual is 0.94 km $\rm s^{-1}$ and csig = 15.18. This indicates that the probability that the presented frequency solution could be generated by noise is 1 in $10^{\rm csig}$. Figure 2(b) plots the residuals after prewhitening. As shown, the residuals are small but not perfectly featureless. To avoid misidentification of true frequencies from aliases, we conservatively discontinued the prewhitening at this step.

Table 2
Rigel Periodocities Found from the Radial Velocity Study

ID	Frequency ($\rm d^{-1}$)	Amplitude (km $\rm s^{-1}$)	$(S/N)_{RV}$	Sig	rms (km $\rm s^{-1}$)
f_1	0.01523 ± 0.00002	1.128 ± 0.027	15.9	105.9	2.189
f_2	0.20635 ± 0.00003	0.964 ± 0.027	14.0	104.4	1.946
f_3	0.19459 ± 0.00003	0.823 ± 0.027	11.8	60.0	1.734
f_4	0.02516 ± 0.00004	0.625 ± 0.027	8.9	46.2	1.617
f_5	0.28297 ± 0.00005	0.562 ± 0.027	8.1	42.8	1.538
f_6	0.06107 ± 0.00003	0.839 ± 0.027	12.0	36.2	1.465
f_7	0.22545 ± 0.00004	0.644 ± 0.027	9.1	32.1	1.399
f_8	0.01338 ± 0.00003	0.839 ± 0.027	11.9	27.7	1.341
f_9	0.31317 ± 0.00004	0.693 ± 0.027	10.0	27.9	1.280
f_{10}	0.17352 ± 0.00005	0.515 ± 0.027	7.5	28.9	1.233
f_{11}	0.09453 ± 0.00005	0.552 ± 0.027	8.0	20.1	1.180
f_{12}	0.15542 ± 0.00006	0.452 ± 0.027	6.5	20.9	1.145
f_{13}	0.04343 ± 0.00006	0.469 ± 0.027	6.7	20.4	1.111
f_{14}	0.13921 ± 0.00004	0.590 ± 0.027	8.6	20.0	1.079
f_{15}	0.12080 ± 0.00005	0.518 ± 0.027	7.5	22.7	1.046
f_{16}	0.82026 ± 0.00007	0.404 ± 0.027	6.4	18.1	1.011
f_{17}	0.36038 ± 0.00008	0.347 ± 0.027	5.0	15.3	0.981
f_{18}	0.31699 ± 0.00007	0.381 ± 0.027	5.5	16.2	0.961
f_{19}	0.51179 ± 0.00009	0.315 ± 0.027	4.7	16.2	0.938

(This table is available in its entirety in machine-readable form in the online journal. A portion is shown here for guidance regarding its form and content.)

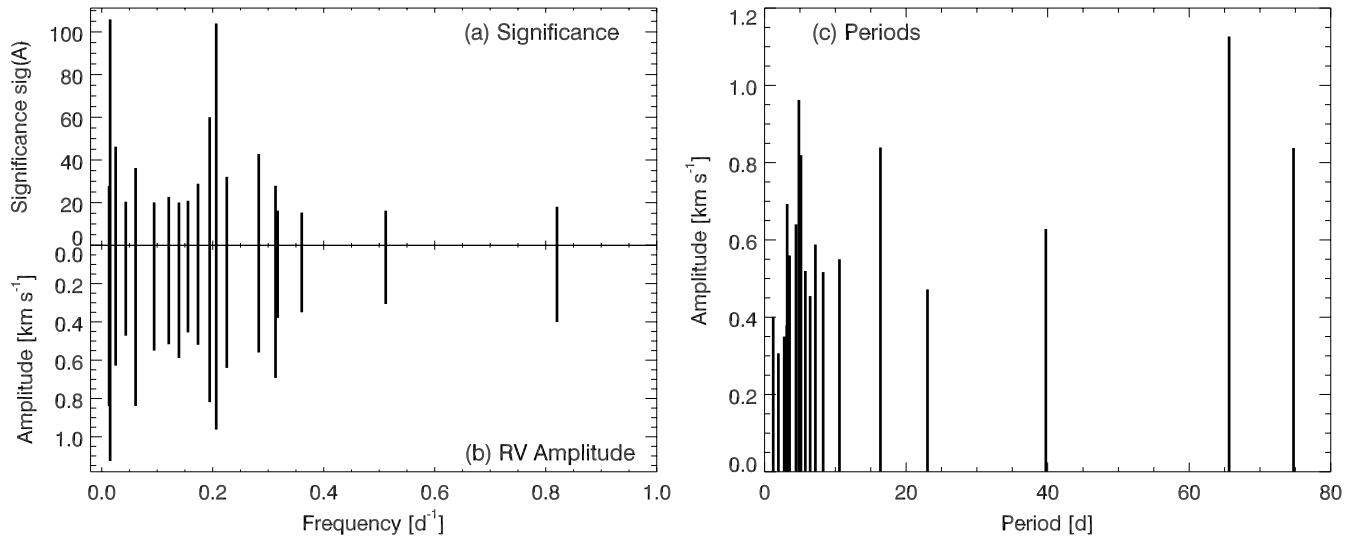

Figure 5. Left: detected frequencies with their corresponding significance level (panel (a)) and radial velocity amplitude (panel (b)). The multimode solution is tabulated in Table 2. Right: period distribution of detected modes with their corresponding amplitude.

4.3. Comparing Results of `SigSpec` *and* `Period04`

A straightforward prewhitening of the data with the same weights used as above with `Period04` starts with the same results as in `SigSpec` for the first few harmonics, but then shows some differences. Instead, we imported the frequencies from the `SigSpec` list and prewhitened sequentially. The maximum difference of 0.01 km s^{-1} between the calculated amplitudes occurs in f_{19}. The final rms of the residual is 0.92 km s^{-1} in `Perod04` and 0.94 km s^{-1} in `SigSpec`. The S/N within a box of 1.0 d^{-1} around f_{19} is 4.70.

4.4. Flux Amplitudes

Independent prewhitening of the *MOST* data set results in tens of modes that have no corresponding counterparts in the frequency list of Table 2. This is quite expected since the baseline of *MOST* observations (∼28 days) is shorter than some of the periods found for the star indicated from the analysis of the RV data. To resolve this, we used the "fixed" frequencies derived from the RV analysis (Table 2) and employed `Period04` to determine the possible corresponding light amplitudes in the *MOST* data. We searched for stable amplitudes and phases (an additional harmonic at the orbital frequency of the satellite $f_{\rm orb} = 14.19827$ d^{-1} was also subtracted). Unfortunately, due to the presence of long-period modes comparable to (and longer than) the *MOST* photometry baseline, no converging solution could be achieved.

4.5. Frequency Distribution of Multimode Solution

According to the asymptotic theory of non-radial stellar oscillations (Tassoul 1980), high-order p and g modes present regularity in frequencies and periods, respectively (Aerts et al. 2010a). In the case of Rigel and similar classes of stars, which are believed to be unstable against g modes, this regularity in period can bring a wealth of information about how stellar material is mixing in the stars' deep interior (see Degroote et al. 2010 for an example). However, as a prerequisite for applying this technique, identification of polar and azimuthal degrees (ℓ, m) for each individual mode is necessary. Unfortunately, the number of secured frequencies is not large enough for a statistical study of any possible period spacings. Moreover, the mode identification is beyond the scope of this paper.

However, after extraction of the frequencies with good precision, it is worthwhile to demonstrate how the modes are distributed according to their corresponding frequencies and amplitudes. For this purpose, the left panel in Figure 5 shows the distribution of detected frequencies between [0, 1] d^{-1} and their corresponding RV amplitudes. Except for f_{16} and f_{19}, the rest of the modes have frequencies below 0.4 d^{-1}. The right panel of Figure 5 shows the corresponding period distribution.

It is possible that the rotation period of Rigel could be detected in the frequency analyses of the RV data. Pápics et al. (2011) found the rotational modulation as the only explanation for the variability in the B0.5 IV *CoRoT* double-line spectroscopic binary HD 51756. Rigel has two modern, self-consistent spectroscopic $v \sin i$ measures (Przybilla et al. 2010; Simón-Díaz et al. 2010) from which we adopt $v \sin i = 25$ km s^{-1}. This $v \sin i$ is typical for a BSG and indicates that an inclination of $i > 60^\circ$ is likely (the inclination i is defined in the usual way as the angle of star's rotation axis relative to our line of sight). Adopting both $i = 60^\circ$ and $i = 90^\circ$ with $R = 78.9\,R_\odot$, yield $P_{\rm rot}(i = 60^\circ) = 137$ d ($\equiv$0.0073 d^{-1}) and $P_{\rm rot}(i = 90^\circ) = 158$ d ($\equiv$0.0063 d^{-1}), respectively. The value of $i > 60^\circ$ is also in accord with the simple angular momentum conservation assumption from the expected $v_{\rm rot} =$ 240–300 km s^{-1} estimated for Rigel when it was an MS O9/B0 V star. As shown in Table 2, there are no significant frequencies in the range of 0.006–0.007 d^{-1}. So, rotation effects can be neglected in our interpretation of frequencies. Yet, we are aware that multiple integers of the rotational frequency might show up in the frequency analysis, and long-period modes could have a non-pulsational origin. Given the weak magnetic field on Rigel, rotational modulations induced by stellar spots are unlikely.

4.6. Frequency Analysis of Equivalent Widths

As panels (c)–(e) in Figure 2 clearly show, Si II λ6347, Si II λ6371, He I 6678, and Hα exhibit the large amplitude changes in EW. However, the binned EW measures have a very low duty cycle and DFT analyses do not lead to any significant frequencies above the 4σ noise threshold. There is only one mode detected for the Si II λ6347 line with frequency, amplitude, and S/N of 0.0336 d^{-1}, 14.71 mÅ, and 4.24, respectively. Similarly for Si II λ6371 line, the only dominant peak in the Fourier power spectrum corresponds to the frequency,

amplitude, and S/N of 0.0336 d^{-1}, 11.32 mÅ, and 3.46, respectively. Therefore, not only do the frequencies from EWs show no apparent correspondences with any of the frequency entries in Table 2, the first two smallest frequencies, i.e., f_8 and f_1, do not appear in the DFT power spectrum of EWs. Hence, with the current time series of spectra at our disposal, we cannot associate the low-frequency range of RV variations with EW variations.

5. SUMMARY

This is the first time that simultaneous space-based photometry and time-resolved medium-resolution optical spectroscopy of a BSG star are presented. Although the short baseline of *MOST* photometry did not enable us to derive flux amplitudes, the long baseline of RV monitoring and the DFT analysis revealed 19 significant modes above S/N = 4.6. These have been shown to arise from non-radial pulsations by Kaufer et al. (1997) with gravity-mode nature (Lefever et al. 2007).

The question of the degree of regularity in light and RV variability in BA supergiants remains unanswered until an uninterrupted long time-baseline space-based observation campaign of these objects is carried out. It is possible that a degree of semi-regularity might exist in the current RV data set. But there is no definite evidence for this, and thus it was not included in our frequency extraction procedure. Therefore, we caution that the periodicities found in our analysis might be affected by this issue. In the near future it will be possible for long-term photometry of Rigel and other bright BSGs to be carried out over several months by the *BRITE-Constellation* Mission (Kuschnig et al. 2009). Observations like these should result in better defined frequencies.

The temporal modulations in the EWs of the two Si II lines show a completely different pattern from those of He Iλ6678 and Hα line, which indicate that EWs formed at different optical depths τ_λ are uncorrelated. This demonstrates that there exists a pulsationally induced non-RV gradient across different optical depths from which the lines are formed (Aerts et al. 2009; Simón-Díaz et al. 2010). As a result, the response of the dilute extended atmosphere of Rigel (which is reminiscent of other BA supergiants) to the pulsational waves emerging from the interior of the star is very complex and has a high potential to probe a wide range of depths where the spectral lines are formed. As shown in Figure 2(d), the EW of the Hα feature shows the largest systematic variations of any of the spectral features measured. Because the Hα feature is also affected by mass outflows/inflows, and winds, it is a difficult line to interpret. It is therefore not surprising that its behavior is different from the other spectral lines studied. A full asteroseismic study of Rigel is planned in a subsequent paper.

We are grateful to the referee, Nancy Morrison, for her valuable comments in improving this paper. E.M. appreciates the hospitality and support he received from Wojcieh Dziembowski during his visit to Nicolas Copernicus Astronomical Center in Warsaw where a part of this study was done; he is also grateful to Patrick Lenz and Eric Chapellier for fruitful discussions on frequency analysis of an uneven sample. We thank Joel Eaton and Frank Fekel for coordinating the AST spectroscopic observations. The research at Tennessee State University was supported in part by NASA, NSF, Tennessee State University, and the state of Tennessee through its Centers of Excellence program. We also thank Jaymie Matthews and the *MOST* team for acquiring and processing the photometry. This work is supported by NASA/MOST grant NNX09AH28G.

Facilities: TSU:AST, *MOST*

REFERENCES

Aerts, C., Christensen-Dalsgaard, J., & Kurtz, D. W. (ed.) 2010a, Asteroseismology (Astronomy and Astrophysics Library; New York: Springer)
Aerts, C., Lefever, K., Baglin, A., et al. 2010b, A&A, 513, L11
Aerts, C., Puls, J., Godart, M., & Dupret, M. 2009, A&A, 508, 409
Aufdenberg, J. P., Ludwig, H.-G., Kervella, P., et al. 2008, in The Power of Optical/IR Interferometry: Recent Scientific Results and 2nd Generation Instrumentation, ed. A. Richichi, F. Delplancke, F. Paresce, & A. Chelli (New York: Springer), 71
Bessell, M. S., Castelli, F., & Plez, B. 1998, A&A, 333, 231
Bresolin, F., Pietrzyński, G., Gieren, W., et al. 2004, ApJ, 600, 182
Chapellier, E., Rodrguez, E., Auvergne, M., et al. 2011, A&A, 525, A23
Chesneau, O., Dessart, L., Mourard, D., et al. 2010, A&A, 521, A5
De Ridder, J., Dupret, M.-A., Neuforge, C., & Aerts, C. 2002, A&A, 385, 572
Degroote, P., Aerts, C., Baglin, A., et al. 2010, Nature, 464, 259
Donati, J.-F., Semel, M., Carter, B. D., Rees, D. E., & Collier Cameron, A. 1997, MNRAS, 291, 658
Dupret, M.-A., De Ridder, J., Neuforge, C., Aerts, C., & Scuflaire, R. 2002, A&A, 385, 563
Dziembowski, W. A., & Slawinska, J. 2005, Acta Astron., 55, 195
Eaton, J. A., & Williamson, M. H. 2007, PASP, 119, 886
Gautschy, A. 2009, A&A, 498, 273
Godart, M., Noels, A., Dupret, M.-A., & Lebreton, Y. 2009, MNRAS, 396, 1833
Heger, A., Woosley, S. E., & Spruit, H. C. 2005, ApJ, 626, 350
Hoffleit, D., & Jaschek, C. (ed.) 1982, The Bright Star Catalogue (Containing Data Compiled through 1979) (4th revised ed.; New Haven, CT: Yale Univ. Observatory)
Israelian, G., Chentsov, E., & Musaev, F. 1997, MNRAS, 290, 521
Kaufer, A., Stahl, O., Wolf, B., et al. 1996, A&A, 305, 887
Kaufer, A., Stahl, O., Wolf, B., et al. 1997, A&A, 320, 273
Kudritzki, R. P., Bresolin, F., & Przybilla, N. 2003, ApJ, 582, L83
Kudritzki, R. P., Puls, J., Lennon, D. J., et al. 1999, A&A, 350, 970
Kudritzki, R. P., Urbaneja, M. A., Bresolin, F., et al. 2008, ApJ, 681, 269
Kuschnig, R., Weiss, W. W., Moffat, A., & Kudelka, O. 2009, in ASP Conf. Ser. 416, Solar-Stellar Dynamos as Revealed by Helio- and Asteroseismology: GONG 2008/SOHO 21, ed. M. Dikpati, T. Arentoft, I. González Hernández, C. Lindsey, & F. Hill (San Francisco, CA: ASP), 587
Lefever, K., Puls, J., & Aerts, C. 2007, A&A, 463, 1093
Lenz, P., & Breger, M. 2005, Commun. Asteroseismol., 146, 53
Maeder, A. (ed.) 2009, Physics, Formation and Evolution of Rotating Stars (Astronomy and Astrophysics Library; Berlin: Springer)
Maeder, A., & Meynet, G. 2011, arXiv:1109.6171
Montgomery, M. H., & Odonoghue, D. 1999, Delta Scuti Star Newsl., 13, 28
Morrison, N. D., Rother, R., & Kurschat, N. 2008, in Clumping in Hot-Star Winds, ed. W.-R. Hamann, A. Feldmeier, & L. M. Oskinova (Potsdam: Univ.-Verl.), 155
Mourard, D., Clausse, J. M., Marcotto, A., et al. 2009, A&A, 508, 1073
Nicolet, B. 1978, A&AS, 34, 1
Pápics, P. I., Briquet, M., Auvergne, M., et al. 2011, A&A, 528, A123
Przybilla, N., Butler, K., Becker, S. R., & Kudritzki, R. P. 2006, A&A, 445, 1099
Przybilla, N., Firnstein, M., Nieva, M. F., Meynet, G., & Maeder, A. 2010, A&A, 517, A38
Reegen, P. 2007, A&A, 467, 1353
Richardson, N. D., Morrison, N. D., Kryukova, E. E., & Adelman, S. J. 2011, AJ, 141, 17
Saio, H. 2011, MNRAS, 412, 1814
Saio, H., Kuschnig, R., Gautschy, A., et al. 2006, ApJ, 650, 1111
Sanford, R. F. 1942, Contributions from the Mount Wilson Observatory, Vol. 661 (Washington, DC: Carnegie Institution of Washington), 1
Shultz, M., Wade, G.A., Neiner, C., et al. 2011, in IAU Symp. 272, Active OB Stars: Structure, Evolution, Mass Loss, and Critical Limits, ed. C. Neiner, G. Wade, G. Meynet, & G. Peters (Cambridge: Cambridge Univ. Press), 212
Simón-Díaz, S., Herrero, A., Uytterhoeven, K., et al. 2010, ApJ, 720, L174
Sterken, C. 1977, A&A, 57, 361
Tassoul, M. 1980, ApJS, 43, 469
U, V., Urbaneja, M. A., Kudritzki, R.-P., et al. 2009, ApJ, 704, 1120
van Leeuwen, F. 2007, A&A, 474, 653
Waelkens, C., Aerts, C., Kestens, E., Grenon, M., & Eyer, L. 1998, A&A, 330, 215
Walker, G., Matthews, J., Kuschnig, R., et al. 2003, PASP, 115, 1023